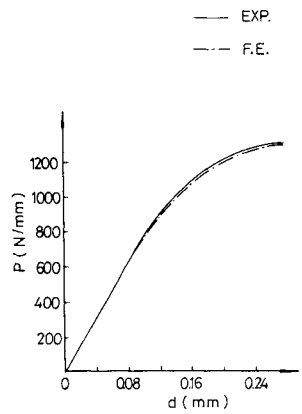

Fig. 4 Load/load line displacement curve.

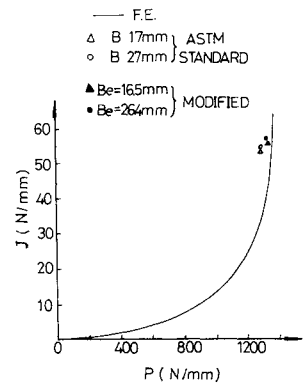

Fig. 5 *J*—*P* relation.

displacement, interelement boundary displacement, and interelement boundary tractions, are assumed. The proper singularities of stresses are embedded in the singular elements, and the interelement compatibility between the singular element and the quadratic isoparametric element is satisfied through the use of a Lagrangian multiplier technique.[3,4] Based on the concept of Saint Venant's principle[5] and numerical experiments, the pin load is treated as a concentrated load. Three integration paths around the crack-tip are selected for computing the J integral and are displayed in Fig. 3. The relations between the applied load and the load line clip gage displacement are described in Fig. 4. The experimental results are in good agreement with those obtained by finite-element analysis. The curve computed by finite-element analysis between the J integral and the applied load per unit thickness of the specimen is illustrated in Fig. 5.

Modification and Discussion

For comparison purposes, the J_{IC} values determined by ASTM standard[2] as seen in Fig. 2 are also shown in Fig. 5. It is noted that those J_{IC} values are determined based on the assumption that the crack-front is located in the area of plane strain situation.[2] However, as shown in Fig. 1, significant plastic deformation or necking without crack extension often occurs on both upper and bottom surfaces. That is, near the upper and bottom surfaces of the specimen, there will be a state of deformation closer to plane stress than plane strain. Hence, the energy required for plastic deformation needs to be taken into account. In order to correct this, the effective thickness B_e is adopted in ASTM standard formulas [e.g., Eqs. (1) and (2)] for calculating J_{IC} values instead of the specimen thickness B. The effective thickness B_e is set equal to the difference between the specimen thickness B and the thickness of plastic deformation. The corrected results are also shown in Fig. 5. As compared with rigorous finite-element solutions, closer J_{IC} values than those obtained from ASTM standard[2] are noted. The numerical-experimental technique established is also demonstrated for other materials with different thicknesses, such as Al-5083-0 alloy. The results are encouraging.

Conclusions

Further studies on the determination of the J_{IC} value using both experimental and finite-element analysis have been successfully made. The effective thickness B_e instead of the specimen thickness B is suggested for ASTM standard formula use. The techniques developed here are useful for determining an accurate J_{IC} value.

References

[1]"Standard Method of Test for Elastic-Plastic Fracture Toughness J_{IC}," JSME Standard S001-1981, pp. 1-31.

[2]"Standard Test Method for J_{IC}, A Measure of Fracture Toughness," ASTM Standard E 813-87, Vol. 03.01, 1988, pp. 686-700.

[3]Atluri, S. N., Nakagaki, M., and Chen, W. H., "Fracture Analysis Under Large-Scale Plastic Yielding: A Finite-Deformation Embedded Singularity, Elastoplastic Incremental Finite Element Solution," *Flow Growth and Fracture,* ASTM STP 1977, pp. 42-61.

[4]Chen, W. H., "Application of Finite Element Method to Elastic—Plastic Fracture Mechanics," *Journal of the Chinese Institute of Engineers,* Vol. 2, No. 1, 1979, pp. 1-13.

[5]Fung, Y. C., *Foundations of Solid Mechanics,* Prentice-Hall, Inc., Englewood Cliffs, NJ, 1965.

Electromagnetic-Capillary Instabilities of Liquid Cylinder: Production of Spherical Shells in Microgravity

Chuen-Yen Chow* and Michael Harvanek†
University of Colorado, Boulder, Colorado

Introduction

HOLLOW metallic spheres have many potential engineering applications. They can be sintered to form lightweight structures of high strength. Spherical shells of submillimeter size are sought as inertial confinement fusion targets. On the other hand, shells filled with gas, liquid, or solid may be used as efficient insulators, explosives, fire retardants, or temperature regulators. Many of the applications rely on great shell precision and smoothness and on the ability to produce large quantities of uniform shells at low cost.

Researchers at the Jet Propulsion Laboratory have been successfully producing spherical shells of various sizes in a ground-based laboratory using a hollow jet instability device[1] in which a molten metal is ejected from an annular nozzle to form a hollow liquid jet. When a flowing gas is passed through the core, the hollow jet becomes unstable and breaks up into drops, which under surface tension will develop into hollow spheres and solidify while moving along a drop tower. The size of the spheres is controlled by adjusting the speed of the core flow.

An alternative method proposed here is to manufacture spherical shells in a low-gravity environment using hollow metallic cylinders placed between two electrodes. When a di-

Presented as Paper 88-3729 at the First National Fluid Dynamics Congress, Cincinnati, OH, July 25-28, 1988; received Aug. 15, 1988; revision received May 22, 1989.

*Professor, Department of Aerospace Engineering Sciences. Associate Fellow AIAA.

†Research Assistant, Department of Aerospace Engineering Sciences.

rect current of high intensity is passed through such a cylinder, it is melted by Joule heating, and the resulting liquid column, which remains the same thickness under the microgravitational condition, is unstable in the presence of both electromagnetic pinch and surface tension, as shown in Fig. 1, and breaks up to form hollow spheres. Without collisions, they become spherical shells of high precision after solidification.

This method utilizing the electromagnetic-capillary instability phenomenon of a hollow liquid column has many advantages. There is no need of furnace or nozzle, and there is no temperature gradient along the column when the material is melted electrically. Uniform shells can be produced from hollow cylinders manufactured with high precision, and the shell size may be controlled by adjusting the applied voltage. Thousands of spheres can be manufactured in a few seconds when a large number of identical metal cylinders are placed between the same pair of electrodes. Provided with a microgravity environment, the operation is much simpler than that for the coaxial jet device in a ground-based laboratory.

Stability Analysis

A stability analysis is carried out for an infinitely long, hollow liquid column, of inner radius R_c and outer radius R_0, that carries an axial electric current of constant density J. The column is initially in static equilibrium, balanced by surface tension, electromagnetic pinch, and the radial pressure difference across the annular region.

In the absence of gravity, the equations governing the motion of an inviscid incompressible fluid of density ρ and constant permeability μ are

$$\mathrm{div}\, V = 0 \tag{1}$$

$$\frac{\partial V}{\partial t} - V \times \mathrm{curl} V = -\mathrm{grad}\left(\frac{p}{\rho} + \frac{V^2}{2}\right) + \frac{\mu}{\rho} J \times H \tag{2}$$

where V is the velocity, p the pressure, H the magnetic field intensity, and J ($=\mathrm{curl} H$) the electric current density. In the laboratory scale, the magnetic Reynolds number is very small, meaning that the electromagnetic field is not influenced by the motion of the conducting fluid. If the variation of H in time is not extremely large, the equation governing the magnetic field is simplified to

$$\mathrm{curl}\ \mathrm{curl} H = 0 \tag{3}$$

For the initial static condition with a uniform axial current, the magnetic field and pressure distribution are computed as functions of radial distance from the axis. The inner and outer surfaces of the column are then perturbed by giving an axisymmetric deformation of the form

$$r_c = R_c + a \exp(ikz + \omega t) \tag{4}$$

$$r_0 = R_0 + b \exp(ikz + \omega t) \tag{5}$$

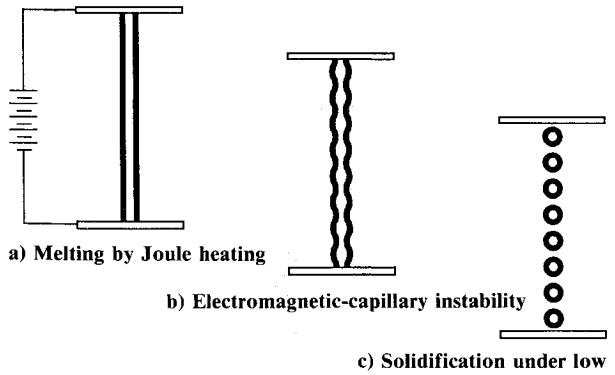

Fig. 1 Suggested electrical device for producing metallic spherical shells.

in which $k = 2\pi/\lambda$ is the wave number, λ being the wavelength of deformation, and a, b are amplitudes of the deformation that are much smaller than the inner radius R_c.

Two different modes of deformation are possible, depending on the signs of a and b. When a and b are of the same sign, the deformation is said to be in sinusoidal mode; otherwise, it is in bubble mode. They are so called because of their respective cross-sectional shapes, sketched in Fig. 2.

The wall deformation causes a perturbation in the electromagnetic field as well as a velocity field in the originally stagnant fluid column. With detailed descriptions available in Ref. 2, the analysis is stated briefly as follows. After electromagnetic fields and flowfields have been computed from Eqs. (1-3), the pressure boundary conditions are applied at the deformed inner and outer surfaces, where the pressure jump is balanced by the normal component of the resultant force due to surface tension T. As a result, a system of two algebraic equations, each containing a and b, is formed. By requiring that the system have a nontrivial solution, a dispersion relation is obtained that has the following dimensionless function form:

$$\Omega^2 = f(G, X_0, N) \tag{6}$$

where $\Omega^2 = \rho\omega^2 R_0^3/T$, $G = R_c/R_0$ is the ratio of inner and outer radii, $X_0 = kR_0$ a nondimensionalized wave number, and $N = \mu J^2 R_0^3/T$ a parameter indicating the relative importance of electromagnetic pinch force as compared with surface tension force.

Results and Discussion

Based on the lengthy expression for f described in Ref. 2, Ω^2 can be plotted as a function of X_0 for given values of G and N. If Ω^2 is positive at a certain value of X_0, ω has a positive real root, which causes the deformation shown in Eqs. (4) and (5) to grow with time. The fluid column thus becomes unstable to disturbance of this particular wavelength. The wavelength to be observed in the laboratory is determined by the value of X_0, at which Ω^2 has a maximum positive value. On the other hand, if Ω^2 is negative, ω has only imaginary parts, so that the initial disturbance will propagate without distortion in the form of traveling waves, corresponding to the state of neutral stability.

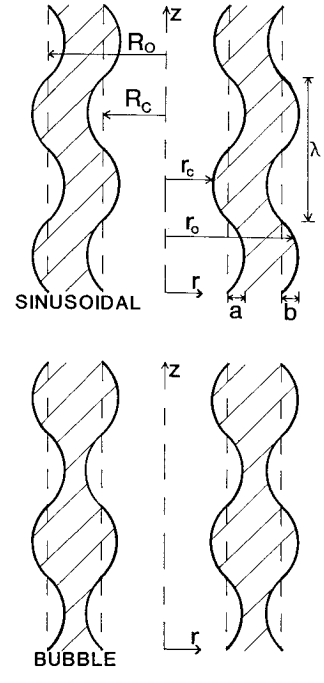

Fig. 2 Two modes of axisymmetric wall deformation.

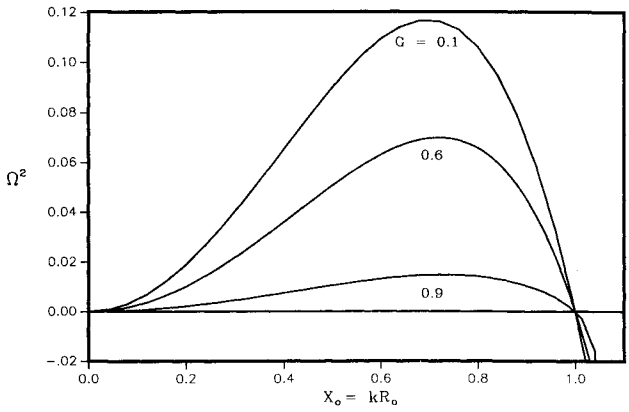

Fig. 3 Growth rate for the bubble mode in nonconducting case $N = 0$.

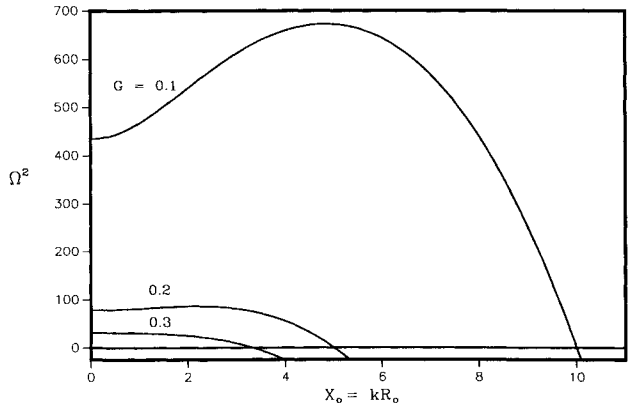

Fig. 4 Growth rate for the sinusoidal mode in nonconducting case $N = 0$.

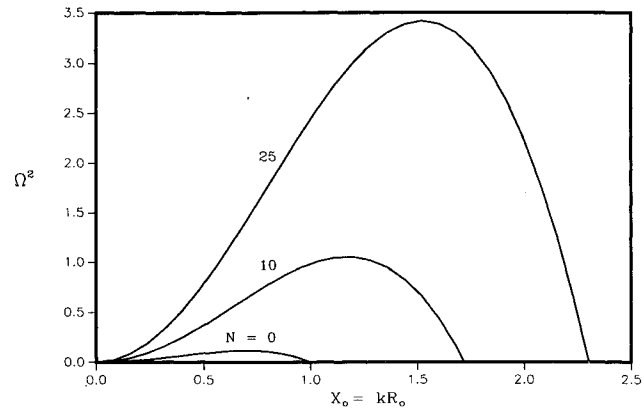

Fig. 5 Growth rate for the bubble mode in the presence of an axial electric current, $G = 0.1$.

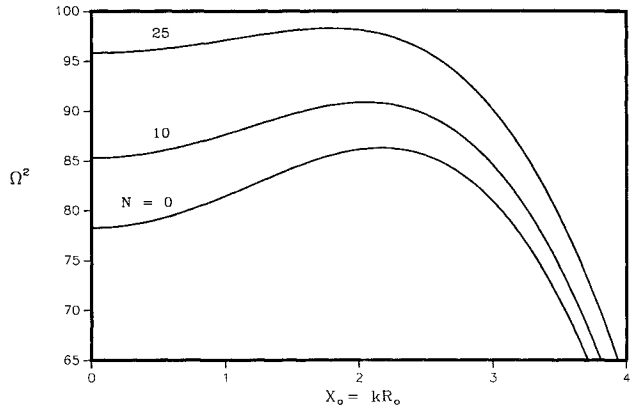

Fig. 6 Growth rate for the sinusoidal mode in the presence of an axial electric current, $G = 0.2$.

The nonconducting case with $N = 0$ is examined first; the results are presented in Fig. 3 for the bubble mode and in Fig. 4 for the sinusoidal mode. The behavior of the bubble mode is similar to that of a liquid cylinder without a core,[3] being always unstable for $0 < X_0 < 1$, regardless of the value of G. In the bubble mode (Fig. 3), as G increases for increasing core size, Ω^2 decreases, so that the system becomes less unstable and the location of Ω^2_{max} shifts toward $X_0 = 1$. On the contrary, behavior of the sinusoidal mode is quite different. Instead of having two zeros at $X_0 = 0$ and 1 for the bubble mode, the growth rate for the sinusoidal mode has only one zero at $X_0 = 1/G$; to the left of the zero, the system is unstable, as shown in Fig. 4. As G increases, the sinusoidal mode becomes less unstable, just like the bubble mode, but the position of Ω^2_{max} moves toward $X_0 = 0$, and the curve flattens. In general, the sinusoidal mode, whose growth rate is several orders higher than that of the bubble mode, is much more unstable.

In the presence of an axial electric current, the sinusoidal mode is still much more unstable than the bubble mode. Some representative results for these two modes are shown in Figs. 5 and 6. Increasing current density enhances instability for both modes and broadens their spectrum of wavelengths for which the column is unstable. However, as N increases, the position of Ω^2_{max} shifts to larger values of X_0 (having shorter wavelengths) for the bubble mode and to the opposite direction for the sinusoidal mode.

In conclusion, regardless of the values of G and N, the sinusoidal mode of deformation is always much more unstable than the bubble mode. Thus, after a hollow metallic cylinder is melted by an axial current, the sinusoidal mode will be amplified much faster. The geometry of the deformation (Fig. 2) will insure that, under surface tension, hollow spheres will result after the pinch-off of the liquid column, as shown in Fig. 1. They solidify without collisions in a microgravity environment to become hollow metallic spheres. For certain core sizes, like the one described by $G = 0.2$, the wavelength of the fastest-growing deformation, or the size of the spheres, can be controlled by varying the current density according to Fig. 6.

There are limitations to this method of making hollow spheres, however. As the core size increases, say for G, from 0.2 (in Fig. 6) to 0.3, Ω^2_{max} for the sinusoidal mode always occurs at $X_0 = 0$ for all values of N (see Fig. 9 in Ref. 2). This result indicates that, for core sizes exceeding a certain limiting value, the liquid column deforms with a very long wavelength so that hollow drops cannot be formed. For this reason, spherical shells produced using the proposed electrical device would have small cores. Furthermore, Fig. 6 shows a slow variation of the position of Ω^2_{max} on the X_0 axis with increasing N, indicating that a small range of spherical sizes can be produced by varying the intensity of the electric current.

The stability analysis presented here is based on an inviscid formulation. It is anticipated that viscosity generally weakens the fluid motion and would therefore have a stabilizing effect. An improved stability analysis to include viscous stresses is still in progress.

Acknowledgments

This research was supported by the Center for Low-Gravity Fluid Mechanics and Transport Phenomena at the University of Colorado, which is funded by the Microgravity Sciences Office of NASA's Office of Space Science and Applications.

References

[1]Lee, M. C., Kendall, J. M., Jr., Bahrami, P. A., and Wang, T. G., "Sensational Spherical Shells," *Aerospace America,* Jan. 1986, pp. 72–76.

[2]Chow, C. Y. and Harvanek, M., "Electromagnetic-Capillary Instabilities of a Hollow Liquid Cylinder: Production of Spherical Shells Under Microgravity Conditions," AIAA Paper 88-3729, July 1988.

[3]Chandrasekhar, S., *Hydrodynamic and Hydromagnetic Stability,* Oxford Univ. Press, London, 1961, pp. 537–538.